# PCCP

**PAPER**

# Influences of molecular packing on the charge mobility of organic semiconductors: from quantum charge transfer rate theory beyond the first-order perturbation†

Guangjun Nan,*[a] Qiang Shi,*[b] Zhigang Shuai[c] and Zesheng Li*[ade]

The electronic coupling between adjacent molecules is an important parameter for the charge transport properties of organic semiconductors. In a previous paper, a semiclassical generalized nonadiabatic transition state theory was used to investigate the nonperturbative effect of the electronic coupling on the charge transport properties, but it is not applicable at low temperatures due to the presence of high-frequency modes from the intramolecular conjugated carbon–carbon stretching vibrations [G. J. Nan *et al.*, *J. Chem. Phys.*, 2009, **130**, 024704]. In the present paper, we apply a quantum charge transfer rate formula based on the imaginary-time flux–flux correlation function without the weak electronic coupling approximation. The imaginary-time flux–flux correlation function is then expressed in terms of the vibrational-mode path average and is evaluated by the path integral approach. All parameters are computed by quantum chemical approaches, and the mobility is obtained by kinetic Monte-Carlo simulation. We evaluate the intra-layer mobility of sexithiophene crystal structures in high- and low-temperature phases for a wide range of temperatures. In the case of strong coupling, the quantum charge transfer rates were found to be significantly smaller than those calculated using the weak electronic coupling approximation, which leads to reduced mobility especially at low temperatures. As a consequence, the mobility becomes less dependent on temperature when the molecular packing leads to strong electronic coupling in some charge transport directions. The temperature-independent charge mobility in organic thin-film transistors from experimental measurements may be explained from the present model with the grain boundaries considered. In addition, we point out that the widely used Marcus equation is invalid in calculating charge carrier transfer rates in sexithiophene crystals.

## I. Introduction

There have been tremendous developments in the last decade in the use of conjugated molecules as active materials in opto-electronic applications, including organic thin-film transistors (OTFTs),[1,2] light-emitting displays,[3] and photo-voltaic cells.[4] The performance of such novel electronic devices made of organic semiconductors depends largely on their ability to efficiently transport charges. Since there are millions of organic candidates that can be made by today's technology, addressing the quantitative structure–function relationship is key to identifying high-performance organic semiconductor materials.[5,6]

Molecular packing is a factor of utmost importance for charge transport properties. The interaction between neigh-boring molecules can vary greatly for different molecular packings, which leads to different transport efficiencies and anisotropies. For example, the oligothiophene crystal struc-tures in the high-temperature (HT) phase are much different from those in the low-temperature (LT) phase.[7] Calculations have shown that mobilities in the HT phase are much larger than those in the LT phase.[8] Another example is tetracene[9,10] and related systems, such as rubrene.[10–13] It has been shown that mobilities of rubrene always exceed those obtained for the

[a] *Institute of Theoretical and Simulational Chemistry, Academy of Fundamental and Interdisciplinary Sciences, Harbin Institute of Technology, 150080 Harbin, People's Republic of China.*
*E-mail: gjnan@hit.edu.cn, zeshengli@hit.edu.cn*
[b] *State Key Laboratory for Structural Chemistry of Unstable and Stable Species, Beijing National Laboratory for Molecular Sciences (BNLMS), Institute of Chemistry, Chinese Academy of Sciences, 100190 Beijing, People's Republic of China.*
*E-mail: qshi@iccas.ac.cn*
[c] *Department of Chemistry, Tsinghua University, 100084 Beijing, People's Republic of China*
[d] *Department of Chemistry, School of Science, Beijing Institute of Technology, 100081 Beijing, People's Republic of China*
[e] *Key Laboratory of Cluster Science of Ministry of Education, Beijing Institute of Technology, 100081 Beijing, People's Republic of China*
† Electronic supplementary information (ESI) available: Direct sampling of discretized Feynman paths; derivation of the charge transfer rate formula with the saddle point approximation from the Fermi gold rule. See DOI: 10.1039/c1cp00001b

unsubstituted tetracene under the same conditions.[10,14] The higher mobilities measured for rubrene were attributed to the different solid-state packing found in both systems.[15] Meanwhile, experiments have shown that the mobilities of rubrene are clearly anisotropic,[12] which is consistent with theoretical calculations that the intermolecular interaction varies in different directions.[14] Usually, the reported mobilities depend strongly on sample preparation and measurement techniques, and thus the actual structure–property relationships are difficult to assess. Therefore computational studies are important to provide a deeper insight into this area.

Previous work has clearly shown that the intermolecular organization in organic semiconductors is intimately dominated by weak van der Waals interactions between adjacent molecules,[16–18] which results in a narrow bandwidth. Furthermore, the mean free path of charge carriers becomes shorter than the lattice constant at high temperature.[19] Thus, it is generally agreed that, at least at room temperature, the charge mobility of semiconducting organic materials is determined by a hopping transport process. Although the experiments have shown that the mobilities behave in a band-like manner at low temperatures in very pure crystals of naphthalene[20] and rubrene,[12,13] theoretical calculations have shown that the band-like temperature-dependence of mobilities can be obtained from hopping model when the nuclear tunneling effect is considered.[14] Hopping transport can be depicted as a charge transfer (CT) reaction in which a charge is transferred from one molecule to the neighboring one. It is also assumed that the charges localize on a molecule long enough so the nuclei relax to their equilibrium geometry, inducing a lattice deformation and forming a polaron. In the semiclassical approximation, or high-temperature limit, Marcus theory has been used extensively to study the influence of crystal structures on the charge mobilities,[8,21–24] and thus two major parameters determine self-exchange CT rates: (i) the electronic coupling (or transfer integral) between adjacent molecules, which needs to be maximized, and (ii) the reorganization energy, which needs to be small for efficient charge transport. The reorganization energy of self-exchange CT reactions in a hole-hopping material is defined as the sum of the geometrical relaxation energies of one molecule upon going from the neutral-state geometry to the charged-state geometry and the neighboring molecule upon going through the inverse process.[25] The electronic coupling is mainly determined by the molecular packing and can vary by several orders of magnitude in organic crystals,[8,21] which may result in the first-order perturbation being invalid in some directions.[26] In ref. 26, a generalized nonadiabatic transition state theory (GNTST) has been applied to investigate the nonperturbative effect of the transfer integrals on the charge transport in oligothiophenes, but the results showed that this semiclassical method is not applicable below room temperature for oligothiophene due to the presence of the high-frequency normal modes from the intramolecular conjugated carbon–carbon stretching vibrations.[8,14,15] How the nonperturbative effect of the electronic coupling influences the charge mobility with temperature is still not clear. Understanding such effects will be helpful to further understand the structure–property relationships and experimental measurements in organic semiconductors. To achieve this goal, more accurate quantum CT rate theories are required.

The rigorous quantum mechanical rate constant has been derived in terms of the time integral of the real-time flux–flux correlation function (FFCF).[27] Considerable progress has been made to compute the real-time FFCF over the last few years.[28–32] The principal theoretical tool used by these and many other authors is the path integral method.[33] One of the main advantages of this approach is the nonperturbative nature of the theory, so that the electronic coupling strength need not be small for its applicability. However, real-time FFCFs are still hard to obtain due to the sign problem.[34] In the literature, a widely used alternative is the analytical continuation approach, where the real-time quantum dynamics is obtained from imaginary time correlation functions, as implemented in a number of quantum, mixed quantum-classical, and semiclassical methods.[35–38] In such a way, the quantum CT rate is expressed by the time integral of the imaginary-time FFCF. Since the CT rates are often dominated by saddle-point trajectories in imaginary time,[37,39] Wolynes proposed that the CT rates can be computed from the stationary phase approximation (SPA) with path integral Monte-Carlo methods.[40] Later, an extended SPA approach was proposed to overcome the inaccuracy of the quadratic expansion in the SPA at low temperatures.[41] The SPA has also been employed in the instanton approach,[37] where Miller and co-workers successfully applied the semiclassical SPA with two dividing surfaces to compute the rate constant, and achieved excellent agreement with the exact results.[42] Thus, the evaluation of imaginary-time FFCF is the key for the CT rate constants. We note that Cao et al. have proposed an effective numerical scheme to compute the FFCF for the two-state CT Hamiltonian.[43] In their work, the FFCF is expressed in terms of vibrational-mode path average, while the path average can be performed by directly sampling paths of the harmonic vibrational modes and then propagating the charge carriers under the influence of harmonic vibrational modes.

In the present paper, our primary interest is to apply a quantum CT rate formula without the assumption of weak electronic coupling to reveal the impact of the electronic coupling, and thus the molecular packing, on charge transport properties as a function of temperature. Oligothiophene is an important organic semiconductor material, and receives wide attention from theoretical[8,44,45] and experimental[7,46,47] viewpoints. In this study, we choose sexithiophene crystals[48,49] as an example to verify the present CT rate theory and explore the influence of molecular packing on charge transport. The reason for choosing sexithiophene is that there are different crystal structures in the HT[48] and LT[49] phases with the same reorganization energy, so the difference in charge transport properties all comes from the molecular packing. Generally speaking, inter-layer electronic couplings are weak in comparison with intra-layer electronic couplings in molecular crystals,[8,26,50] and have negligible influence on the charge transport within the intra-layer plane. Therefore, the present work only deals with two-dimensional (2D) charge transport properties.

The paper is organized as follows. In section II, we derive the quantum CT rate formula as a function of the imaginary-time

FFCF and elucidate the numerical scheme of Cao *et al.*[43] for computing the imaginary-time FFCF. In section III, we present the calculation methods for the intra- and inter-molecular parameters required in the CT rate formula and the mobility of charge carriers. Section IV gives the numerical results and discussion. Conclusions are drawn in section V.

## II. Methodology

### A. Spin-boson Hamiltonian

In semiconducting organic materials, the electronic energy difference between two electronic states for the self-exchange CT reaction is zero.[8,21,23,24] We first assume that the potential energy surfaces on the donor and acceptor states can be described by a shifted harmonic oscillator model, and $\{\omega_j\}$ and $\{\lambda_j\}$ are the frequencies and reorganization energies of intramolecular normal modes, respectively. The Hamiltonians of donor and acceptor states can then be written as[26,51]

$$H_1 = \sum_{j=1}^{N} \frac{p_j^2}{2m_j} + \sum_{j=1}^{N} \frac{1}{2} m_j \omega_j^2 \left( x_j - \frac{1}{2} x_{0j} \right)^2 \qquad (1)$$

and

$$H_2 = \sum_{j=1}^{N} \frac{p_j^2}{2m_j} + \sum_{j=1}^{N} \frac{1}{2} m_j \omega_j^2 \left( x_j + \frac{1}{2} x_{0j} \right)^2, \qquad (2)$$

with

$$x_{0j} = \frac{1}{\omega_j} \sqrt{\frac{2\lambda_j}{m_j}}. \qquad (3)$$

Here, $N$ is the number of intramolecular vibrational modes, $x_j$ and $p_j$ are the position and momentum of the $j$-th normal mode with mass $m_j$, $\omega_j$ and $\lambda_j$ are the frequency and reorganization energy of the $j$-th normal mode, respectively. It is useful to define $c_j^2 = \frac{1}{2} m_j \omega_j^2 \lambda_j$, and the Pauli matrices $\sigma_z = |1\rangle\langle 1| - |2\rangle\langle 2|$ and $\sigma_x = |1\rangle\langle 2| + |2\rangle\langle 1|$. Next, we assume that $V$ is the electronic coupling between the donor and acceptor states, and the system can then be described by a spin-boson Hamiltonian:

$$H = V\sigma_x + \sum_{j=1}^{N} \left[ \frac{p_j^2}{2m_j} + \frac{1}{2} m_j \omega_j^2 \left( x_j - \frac{c_j}{m_j \omega_j^2} \sigma_z \right)^2 \right]. \qquad (4)$$

This is the primary model for investigating nonadiabatic transitions because of its physical richness,[52] and has been widely applied to investigate two-state CT reactions.[53–55]

### B. Charge transfer rate

The rigorous quantum mechanical rate constant is given by the time integral of the real-time FFCF,[27]

$$k = \frac{1}{2Z_1} \int_{-\infty}^{\infty} dt \, \text{Tr}[e^{-\beta H} e^{iHt/\hbar} F e^{-iHt/\hbar} F]. \qquad (5)$$

Here, $H$ is the total Hamiltonian and has the form of eqn (4) in the present paper, $F = (i/\hbar)[H,h]$ is the operator of flux, $h = |2\rangle\langle 2|$ is the acceptor state population, $Z_1 = \text{Tr}[e^{-\beta H}(1 - h)]$ is the partition function of the donor state, and $\beta = 1/k_B T$ where $T$ is the temperature and $k_B$ is the Boltzmann constant.

From the spin-boson Hamiltonian, eqn (4), the flux operator can be simplified as $F = -V\sigma_y/\hbar$ with Pauli matrix $\sigma_y = i(|2\rangle\langle 1| - |1\rangle\langle 2|)$. The partition function of the acceptor state has the form $Z_2 = \text{Tr}[e^{-\beta H}h]$. For the self-exchange CT reactions, we have $Z_1 = Z_2$. Eqn (5) is then written as

$$k = \int_{-\infty}^{\infty} dt \, C_{ff}(t), \qquad (6)$$

where the real-time FFCF $C_{ff}(t)$ is defined as

$$C_{ff}(t) = \frac{V^2}{\hbar^2 Z} \text{Tr}[e^{-\beta H} e^{iHt/\hbar} \sigma_y e^{-iHt/\hbar} \sigma_y] \qquad (7)$$

with $Z = 2Z_1 = Z_1 + Z_2 = \text{Tr}[e^{-\beta H}]$.

It has been shown that the CT rates are often dominated by stationary phase point trajectories in imaginary time.[37,39,42] One of these stationary phase points generally occurs at a pure imaginary time in the interval 0 to $i\beta\hbar$,[40] which is called the dominant saddle point ($\tau_{st}$). The integral in eqn (6) can then be calculated over a shifted time line $t' = \tau_{st} + t$:

$$k = \int_{\tau_{st}-\infty}^{\tau_{st}+\infty} dt \, C_{ff}(\tau_{st} - t). \qquad (8)$$

To proceed, we introduce Wick's rotation $t \to -i\tau$, then the eqn (8) in terms of time integral of the real-time FFCF becomes the imaginary part of the integral of the imaginary-time FFCF

$$k = \text{Im} \int C_{ff}(\tau_{st} + i\tau) \, d\tau, \qquad (9)$$

and the real-time FFCF becomes the imaginary-time FFCF,

$$C_{ff}(\tau) = \frac{V^2}{\hbar^2 Z} \text{Tr}\left[ e^{-(\beta\hbar - \tau)H/\hbar} \sigma_y e^{-\tau H/\hbar} \sigma_y \right]. \qquad (10)$$

Further approximation is needed to calculate the integral in eqn (9), which is the imaginary part of a diverging integral. This can be done by using the saddle point approximation,[40,56–58] so we write the imaginary-time FFCF as $C_{ff}(\tau_{st} + i\tau) = e^{-\phi(\tau_{st} + i\tau)}$ and expand $\phi(\tau_{st} + i\tau)$ at the dominant saddle point $\tau_{st}$, giving

$$\phi(\tau_{st} + i\tau) \approx \phi(\tau_{st}) - \frac{1}{2}\phi''(\tau_{st})\tau^2. \qquad (11)$$

It is easy to show that if $\phi''(\tau_{st}) = C_{ff}''(\tau_{st})/C_{ff}(\tau_{st})$, then the quantum CT rate constant is given by[36]

$$k = C_{ff}(\tau_{st}) \sqrt{\frac{2\pi}{C_{ff}''(\tau_{st})/C_{ff}(\tau_{st})}}. \qquad (12)$$

It is obvious that the imaginary-time FFCF at $\tau_{st}$ has to be evaluated before the CT rate is obtained. The next subsection will show how to calculate the imaginary-time FFCF.

### C. Path integral Monte-Carlo route for imaginary-time flux–flux correlation function

The spin-boson Hamiltonian in eqn (4), can be separated into three parts

$$H = H_0 + H_{vib} + H' + \text{const.}, \qquad (13)$$

where

$$H_0 = V\sigma_x \qquad (14)$$

is the Hamiltonian describing the electronic states of the charge carriers,

$$H_{\text{vib}} = \sum_{j=1}^{N} H_{\text{vib}}^{j} = \sum_{j=1}^{N} \left( \frac{p_j^2}{2m_j} + \frac{1}{2} m_j \omega_j^2 x_j^2 \right) \qquad (15)$$

is the Hamiltonian of intramolecular vibrational modes, and

$$H' = -\sum_{j=1}^{N} c_j x_j \sigma_z \qquad (16)$$

is the coupling between charge carriers and intramolecular vibrational modes. When the quantity of interest, $F$, is a function of the electronic degree of freedom only, Cao et al. has expressed this quantity at real time $t$ in terms of vibrational-mode path average.[43] When Wick's rotation has been introduced, this quantity can be expressed as path integration over imaginary time $\tau$,

$$\langle F[x(\tau)] \rangle_{\text{vib}} = \frac{\int dx \int Dx(\tau) F[x(\tau)] e^{-S_\beta[x(\tau)]/\hbar}}{\int dx \int Dx(\tau) e^{-S_\beta[x(\tau)]/\hbar}}, \qquad (17)$$

where $x(0) = x$, $x(\beta\hbar) = x$ and $S_\beta[x(\tau)]$ is the imaginary-time action functional.[59] Based on eqn (17), the imaginary-time FFCF is written as[43]

$$C_{\text{ff}}(\tau)$$
$$= \frac{V^2}{\hbar^2} \frac{\left\langle \text{Tr}\left[\exp\left(-\int_0^{\beta\hbar-\tau} du\, H(u)/\hbar\right)\sigma_y \exp\left(-\int_0^{\tau} du\, H(u)/\hbar\right)\sigma_y\right]\right\rangle_{\text{vib}}}{\left\langle \text{Tr}\left[\exp\left(-\int_0^{\beta\hbar-\tau} du\, H(u)/\hbar\right) \exp\left(-\int_0^{\tau} du\, H(u)/\hbar\right)\right]\right\rangle_{\text{vib}}}. \qquad (18)$$

In the above equation, $H(u) = H_0 + H'[x(u)]$ is imaginary-time dependent Hamiltonian of charge carriers evolving under the influence of the harmonic vibrational modes.

Since the imaginary-time action is quadratic and thus the functional integrand of eqn (17) in discretized form is a multidimensional Gaussian function, the vibrational-mode path average can be performed by direct Monte-Carlo sampling. To achieve this, the first step is to obtain the terminal points of all the vibrational modes. For the $j$-th mode, the terminal points can be easily sampled from the quadratic action,

$$\exp\{-S_\beta(x_j)/\hbar\}$$
$$= \exp\left\{-\frac{m_j\omega_j}{2\hbar\sinh(\beta\hbar\omega_j)}\left[(x_1^2+x_2^2)\cosh(\beta\hbar\omega_j)-2x_1 x_2\right]\right\}\Big|_{x_1=x_2=x_j}$$
$$= \exp\left\{-\frac{m_j\omega_j}{\hbar}\tanh\left(\frac{1}{2}\beta\hbar\omega_j\right)x_j^2\right\}. \qquad (19)$$

The next step is to sample the intermediate time slices of the discretized Feynman paths. Let us define $N$-dimensional vectors $|x_0\rangle = |x_0^1 \cdots x_0^N\rangle$ and $|x_\tau\rangle = |x_\tau^1 \cdots x_\tau^N\rangle$ with $x_0^j$ and $x_\tau^j$ being the two terminal points of the $j$-th vibrational-mode paths. It should be noted that $x_0^j$ and $x_\tau^j$ are equivalent and can be sampled from eqn (19). The imaginary time propagator,

whose details are given in Appendix A (see the ESI†), has the following form

$$\left\langle x_\tau \left| \exp\left(-\tau\frac{H_b}{\hbar}\right) \right| x_0 \right\rangle = \Gamma(\{m_j, \bar{\omega}_j, x_0^j, x_\tau^j\})$$
$$\times \prod_{l=1}^{P-1} \int da_l \exp\left\{-\frac{1}{2}\omega_l^2 a_l^2\right\}. \qquad (20)$$

The set $\{a_l\}$ can be easily sampled from the Gaussian distribution in eqn (20). The imaginary-time FFCF can then be obtained with the description in Appendix A.

## III. Computational details

### A. Modeling intra- and intermolecular parameters

The frequencies and reorganization energies of the intramolecular normal modes can be computed through normal-mode analysis.[5,6,8,14,26,60] Within this approach, the geometries of the neutral and charged molecules are first fully optimized quantum chemically and the normal modes are calculated at the equilibrium structures. Then the changes in geometry between the neutral and charged states are projected onto all the normal modes.[61] Finally, the reorganization energy related to the $j$-th vibrational mode can be calculated by $\lambda_j = k_j \Delta Q_j^2 / 2$, where $\Delta Q_j$ represents the displacement along the normal mode $j$ between the equilibrium geometries of the neutral and charged molecules (Fig. 1) and $k_j$ is the corresponding force constant. In practice, the reorganization energies can be obtained through the DUSHIN program developed by Reimers.[61] The geometry optimization and the normal-mode analysis were carried out at density functional theory (DFT) level by using the hybrid Becke 3-parameter functional for exchange plus the Lee–Yang–Parr correlation functional (B3LYP) with the 6-31G* basis set. The next step is to calculate the intermolecular electronic coupling term. Several methods have been proposed in the literature, e.g., energy level splitting,[23,62] minimized energy level splitting along the reaction path,[63] site-energy corrected coupling[64] and direct evaluation.[8,65,66] The benchmark study of the performance
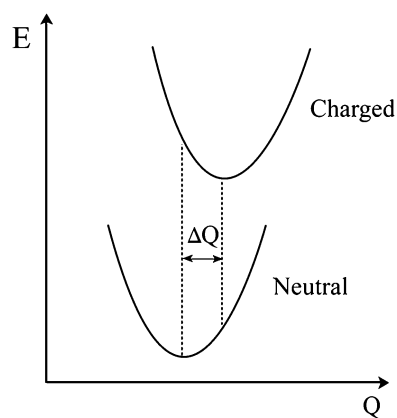


**Fig. 1** Schematic representation of the potential energy surfaces of the neutral and charged molecules. $\Delta Q$ is the normal mode displacement.

using these methods has been given elsewhere.[26] It has been found that the last three methods give very similar results. In this work, we use the direct evaluation method to calculate the hole transfer integral:

$$V = \langle \phi_{HOMO}^{0,site1} | F | \phi_{HOMO}^{0,site2} \rangle, \qquad (21)$$

where $\phi_{HOMO}^{0,site1}$ and $\phi_{HOMO}^{0,site2}$ are the highest occupied molecular orbitals (HOMOs) of the two adjacent molecules 1 and 2 when no intermolecular interaction is present. $F$ is the Fock operator and its density matrix is constructed from noninteracting molecular orbitals:

$$F = SC\varepsilon C^{-1}. \qquad (22)$$

Here, $S$ is the intermolecular overlap matrix, $C$ and $\varepsilon$ are molecular orbital coefficients and energies from one-step diagonalization without iteration. The PW91 exchange and PW91 correlation functionals plus a 6-31G$^*$ basis set are employed. It has been shown that this choice can give the best description for electronic coupling at the DFT level.[67] All DFT calculations for intra- and intermolecular parameters were performed with GAUSSIAN 03 package.[68]

### B. Propagation of charge carriers and evaluation of charge mobilities

Given the quantum CT rates, the charge mobilities may be obtained by assuming a Brownian motion of the charge carriers in the absence of applied electric fields and using the Einstein relation $\mu = eD/k_B T$.[8,14,69] The diffusion coefficient $D$ is evaluated with a set of kinetic Monte-Carlo (KMC) simulations through 2D molecular layer structure.[14,60] We randomly choose one molecule in one molecular layer as the starting point. In each KMC simulation, a single charge carrier moves in the layer *via* hopping events occurring between nearest-neighbor molecules with a probability $p_n = \left( k_n \Big/ \sum_m k_m \right)$ for the $n$-th pathway, where the summation in the denominator runs over all the pathways in 2D molecular layer. The hopping time is $1/k_n$ and the hopping distance is taken to be the molecular center–center distance. At each step, a random number $r$ uniformly distributed between 0 and 1, is generated. If $\sum_{n=1}^{j-1} p_n < r \le \sum_{n=1}^{j} p_n$, then the charge is assumed to propagate along the $j$-th direction. The simulation continues until the total simulation time is achieved. We save the squared displacement every 100 ns and choose the total simulation time for each KMC to be 10 μs. Such simulations are repeated to get thousands of independent charge diffusion trajectories until the averaged squared displacement $l(t)^2 = \frac{1}{K} \sum_{i=1}^{K} l_i(t)^2$ reaches an approximately linear function of simulation time $t$ (Fig. 2) where $l_i(t)$ is the transport distance for the $i$-th trajectory at time $t$ and $K$ is the number of trajectories. In the present paper, 2000 trajectories are performed to achieve the averaged squared displacement. The diffusion coefficient is then evaluated as $D = \lim_{t \to \infty} (l(t)^2/4t)$ and the charge mobility is obtained from the Einstein relation. The statistical error estimate is required and a simplified process has been proposed in previous work.[8,14] In the present paper, some of the electronic couplings are large, such that the first-order
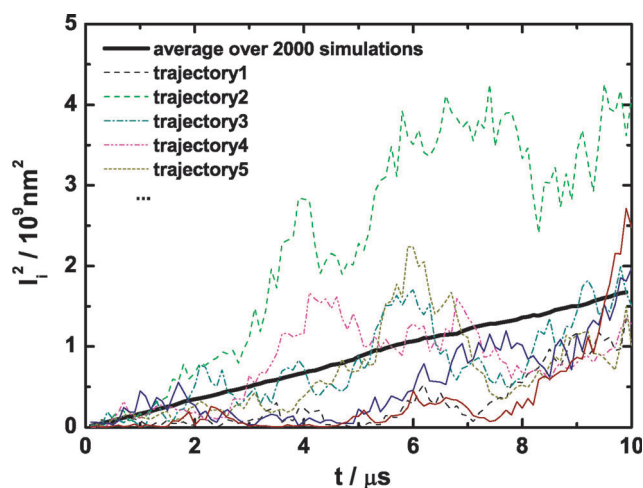


**Fig. 2** Squared displacement $l_i(t)^2$ *versus* simulation time for a 2D sexithiophene layer at room temperature. Each thin line represents an individual trajectory of the kinetic Monte-Carlo simulations. The thick solid line is the average over 2000 simulations.

perturbation is no longer valid. However, the carrier mobility can always be obtained from the above description as long as the CT rates still exists.

## IV. Results and discussion

Sexithiophene exhibits a herringbone structure in the crystal form. However, depending on the sublimation temperatures, there exist two different types of structures, which are shown in Fig. 3. It is clear that the two crystal forms differ in the number of molecules in the unit cell: there are two molecules in one unit cell for the HT-grown crystal while there are four molecules in one unit cell for the LT phase. Another difference is that the inversion center of the centrosymmetric molecule
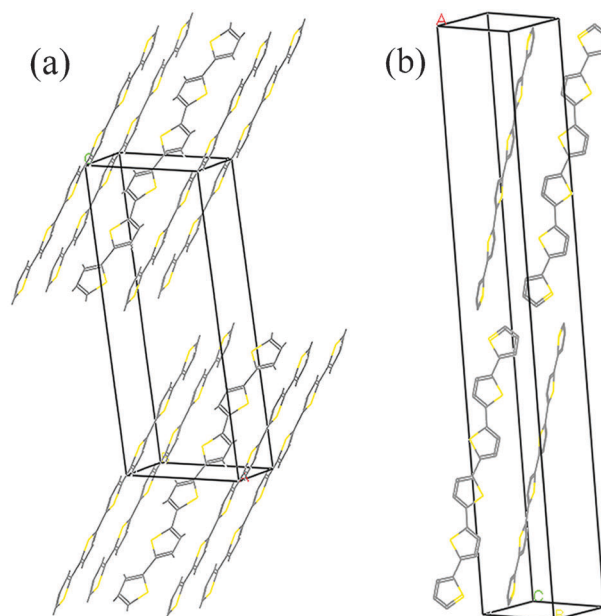


**Fig. 3** Crystal structures of sexithiophene: (a) the unit cell of the HT phase; (b) the unit cell of the LT phase.
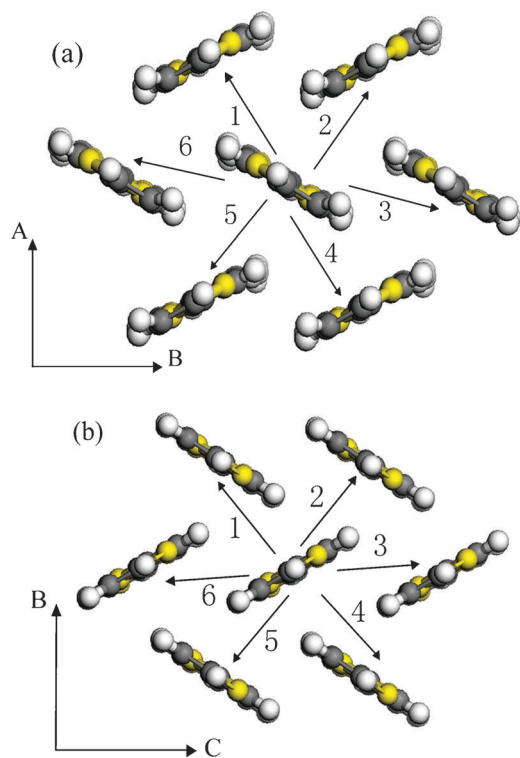
**Fig. 4** Charge hopping pathways in a 2D layer for sexithiophene: (a) the pathways of the crystal structure in the HT phase; (b) the hopping routes of the crystal structure in the LT phase.

does not coincide with a center of symmetry of the lattice in the HT form, whereas it does in the LT form.[7] It has been shown that the organic active layer in OTFTs is an approximately 2D structure;[71,72] the 2D charge transport pathways in a molecular monolayer for the HT and LT phases are shown in Fig. 4. The corresponding intermolecular center-to-center distances and the transfer integrals are given in Table 1. It is clear that the pathways along 1, 2, 4, and 5 in the HT phase are more symmetric than those in the LT phase. While the center-to-center distances of these pathways are larger for the HT phase than those for the LT phase, the former transfer integrals are larger than the latter. For pathways 3 and 6, the case is opposite. The distances along these two pathways are smaller in the HT phase than those in the LT phase, but the former transfer integrals are smaller than the latter. These results can be understood from molecular packing. For pathway 5, we can see that there is a displacement of about one

**Table 1** Intermolecular center-to-center distances and corresponding transfer integrals of the nearest neighbors in one molecular layer for the sexithiophene HT phase and LT phase at DFT level with PW91 exchange and PW91 correlation functionals plus a 6-31G* basis set

| | HT | | LT | |
|---|---|---|---|---|
| Pathway | $d$ (Å) | $V$ (meV) | $d$ (Å) | $V$ (meV) |
| 1 | 5.382 | 36.03 | 4.975 | 18.43 |
| 2 | 5.382 | 36.04 | 4.925 | 15.68 |
| 3 | 5.684 | 3.35 | 6.029 | 10.39 |
| 4 | 5.382 | 36.03 | 4.925 | 15.67 |
| 5 | 5.382 | 36.05 | 4.975 | 18.43 |
| 6 | 5.684 | 3.35 | 6.029 | 10.39 |
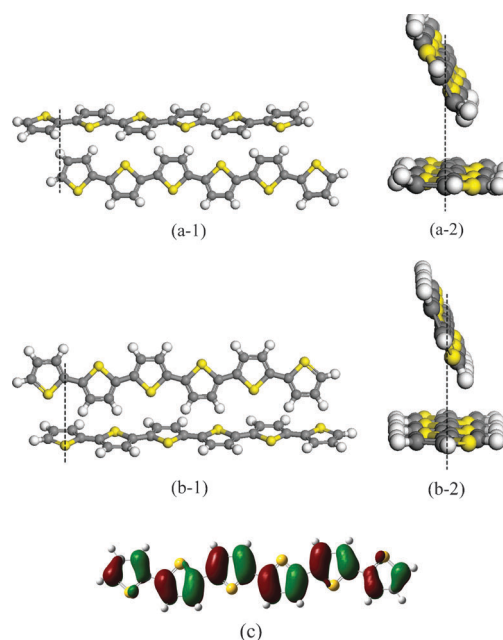


**Fig. 5** Intermolecular displacement taken from crystal packing along the long and short molecular axes for pathway 5: (a-1) and (a-2) for HT phase; (b-1) and (b-2) for LT phase. (c) The molecular HOMO. By symmetry, the molecular packing along pathways 1, 2 and 4 is the same as 5. The dashed line is intended simply as a guide to the eye.

thiophene ring along the long molecular axis in Fig. 5(a-1) for the HT phase, while for the LT phase, the displacement is about half a thiophene ring width in Fig. 5(b-1). Meanwhile, there is little displacement along the short molecular axis for the two phases, as seen in Fig. 5(a-2) and Fig. 5(b-2). It has been noted that the transfer integral is large if the HOMOs of adjacent molecules are fully bonding or antibonding, and can be decreased when mixing occurs between bonding and antibonding overlaps.[5] From the HOMO wavefunction of sexithiophene in Fig. 5(c), we can conclude that the displacement of about one thiophene ring can yield a bonding or antibonding interaction, while the displacement of about half a thiophene ring can mix the bonding and antibonding interactions, which leads to a larger transfer integral along pathway 5 in the HT phase than that in the LT phase. The situation is the same for pathways 1, 2 and 4 as pathway 5. For pathway 3, Fig. 6 shows that there is little displacement along the long molecular axis between the neighboring molecules in the HT phase and there is a displacement of about one thiophene ring along the long molecular axis in the LT phase. The bonding or antibonding interaction is present in each case. However, the displacement along the short axis in the HT phase is larger than that in the LT phase, which reduces the overlap of the wavefunctions between adjacent molecules. Thus, the transfer integral along pathway 3 is larger in the LT phase than that in the HT phase. The molecular packing along pathway 6 is similar to pathway 3. We will see below that the different molecular packings in the crystal structures leads to different charge transport properties.

The imaginary-time FFCF is required to obtain the CT rates. The normal modes evaluated from section III.A are used for the Gaussian samplings in eqn (19) and (20). When the end
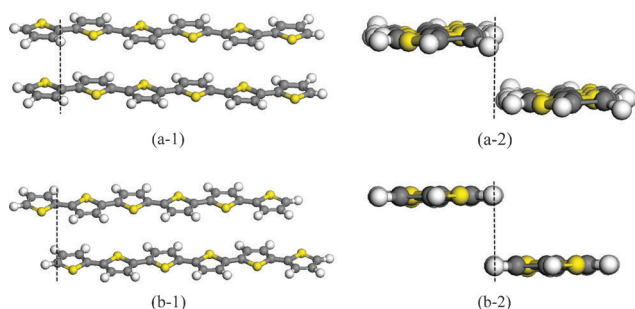
**Fig. 6** Intermolecular displacement taken from crystal packing along the long and short molecular axes for pathway 3: (a-1) and (a-2) for HT phase; (b-1) and (b-2) for LT phase. By symmetry, the molecular packing along pathway 6 is the same as 3. The dashed line is intended simply as a guide to the eye.

points have been sampled for all the vibrational modes, the imaginary-time interval from 0 to $i\beta\hbar$ is divided into $P = 100$ time slices, and the eqn (A17) in Appendix A is computed in each time slice. In this study, 10 000 groups of the samplings are adopted for the vibrational-mode path average in eqn (18) to obtain the imaginary-time FFCF. 1000 such calculations are performed to make sure that the error estimate $\delta$ in Appendix A is small enough ($\delta < 10^{-3}$) near $\tau_{st}$, and then the average of the 1000 FFCFs is used in further calculations. Fig. 7 shows the average imaginary-time FFCFs along pathways 3 and 5 of Fig. 4(a) which correspond to the smallest and largest transfer integrals in Table 1. We can see the dominant saddle point $\tau_{st}$ occurs at $i\beta\hbar/2$. The FFCFs become flatter near the stationary point with decreasing temperature. The FFCFs also become deeper with the increase of the transfer integral for the same temperature. It should be pointed out that the present method is only valid when the charge carriers are localized and the CT dynamics is a rate process. This assumption requires a sufficiently high energy barrier between the neighboring molecules, which could become invalid for high-mobility semiconductors where the electronic coupling is comparable or larger than the reorganization energy. As long as the hopping picture holds, the FFCFs can be used in eqn (12) to compute the CT rates and then the mobilities. It
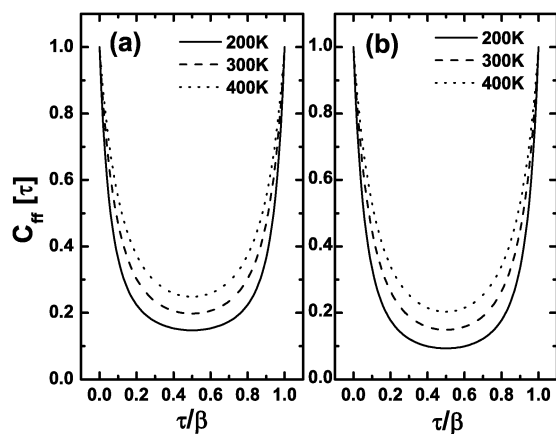
has been noted that the energy barrier can exist when the reorganization energy is larger than the four times the largest electronic coupling for the self-exchange CT reactions.[5,14] For the present study, the reorganization energy of sexithiophene is about 240 meV,[8] which is much larger than four times the largest electronic coupling in Table 1. Thus, the hopping picture is valid, and we can safely employ the average imaginary-time FFCFs at $\tau_{st}$ to compute the quantum CT rates in eqn (12).

Before showing the results for CT rates from eqn (12), we need to estimate the error introduced from the SPA. To achieve this, we made the SPA for the CT rate formula from the Fermi golden rule (FGR) to get an analytic CT rate formula (FGR-SPA) in Appendix B (see the ESI†). The comparison between FGR and FGR-SPA is shown in Fig. 8. We can see that the FGR-SPA results are almost parallel to the FGR results along various transport directions in the HT phase, and the SPA introduces about 20% error in the investigated temperature region. This is consistent with the conclusion of Miller *et al.*[42] that about 20% error is introduced from the SPA for the thermal rate constants. The comparison between FGR and FGR-SPA results in the LT phase is similar to that in HT phase and is not given here. Then the SPA approximation is likely to be applicable to study the nonperturbative effect of strong electronic couplings, although its accuracy may need to be further tested in future studies.

Fig. 9 compares the present results with those from the FGR-SPA formula along the pathways of the sexithiophene crystal structure in the HT phase. The results from the GNTST[51] are also shown. We can see clearly in Fig. 9(a) that the present CT rates are consistent with the FGR-SPA results. This shows that the present theoretical methodology can recover the FGR-SPA formula under the weak electronic coupling limit, so the first-order perturbation is applicable along pathway 3 of the HT phase, which agrees with our previous conclusion.[26] While the GNTST results are similar to the present results, it should be noted that the GNTST results increase more rapidly with decreasing temperature below 300 K, and even exceed the present results. This is due to
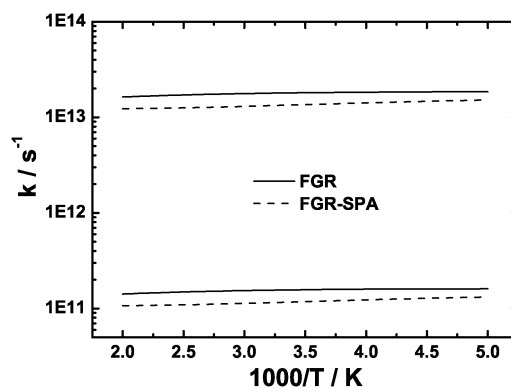


**Fig. 8** The comparison of the CT rates from eqn (B1) and (B10) in Appendix B along the pathways 3 and 5 in the HT-phase sexithiophene crystal structure: the bottom pair of lines is for pathway 3, and the top pair is for pathway 5. The solid line is the FGR results and the dash line is the FGR-SPA results. By symmetry, pathways 1, 2 and 4 are the same as 5, and 3 is the same as 6.



**Fig. 7** The average imaginary-time flux–flux correlation function along pathways 3 and 5 in the HT-phase sexithiophene crystal structure at different temperatures: (a) for pathway 3; (b) for pathway 5.
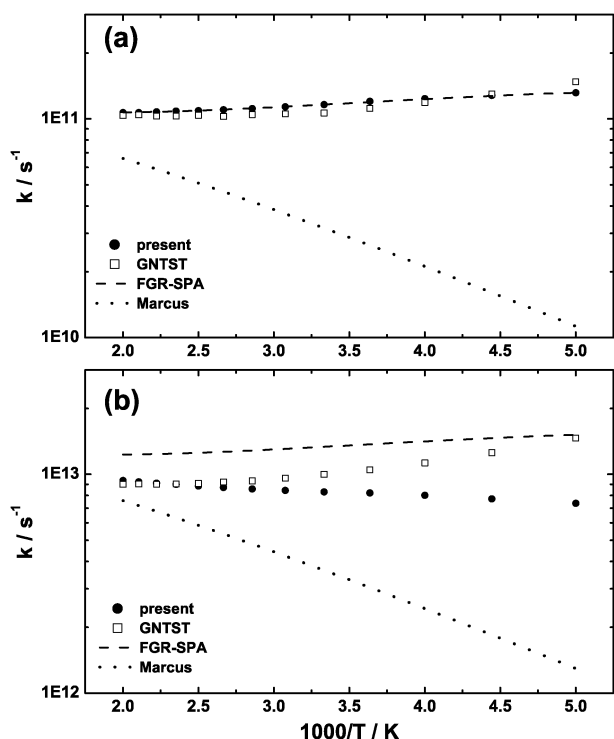
**Fig. 9** The CT rates along pathways 3 and 5 of the HT- phase sexithiophene crystal structure: (a) for pathway 3; (b) for pathway 5. The solid circle represents the present results; the hollow square represents the GNTST results; the dashed line represents FGR-SPA results; the dotted line represents the Marcus results. By symmetry, pathways 1, 2 and 4 are the same as 5, and 3 is the same as 6.

the fact that the quantum correction of partition function in GNTST is derived semiclassically[70] and is overestimated below room temperature for sexithiophene. When the electronic coupling becomes larger, this overestimation for the quantum correction of partition function in GNTST can make a much larger difference when comparing with the present results, as seen in Fig. 9(b). It is clear that the GNTST results are similar to the present results above 400 K. As the temperature decreases, the GNTST results increase much more rapidly and can no longer predict the correct CT rates for sexithiophene below room temperature. In addition, Bader and co-workers have also used eqn (12) to satisfactorily investigate the role of nuclear tunneling in a CT process.[36] Thus, the present method can predict the charge transport properties in organic semiconductors more accurately over a wider range of temperature. Comparing the present and the FGR-SPA results, we can see in Fig. 9(b) that the former are obviously lower than the latter, especially in the low-temperature region. This can be attributed to the nonperturbative effect of the strong electronic coupling. It is also surprising that the present results are reduced with decreasing the temperature – the opposite of the FGR-SPA results. Thus, the first-order perturbation cannot predict correct charge transport properties along this pathway. The nonperturbative effect of the transfer integral can change the CT rates *versus* temperature dramatically when the electronic coupling is large enough. For the LT phase, we can see in Fig. 10 that the first-order perturbation is approximately applicable along

pathways 3 and 6, but becomes less accurate along pathways 1, 2, 4 and 5, although the difference between the present results and the FGR-SPA results is not very large. As the transfer integrals increase, the present results gradually become smaller than the FGR-SPA results, and the first-order perturbation gradually becomes invalid. Comparing all of the present and the FGR-SPA results in Fig. 9 and 10, we conclude that the larger the electronic coupling, the more the present CT rate decreases comparing with the results from first-order perturbation, which is also consistent with our previous calculation.[26] Since the semiclassical Marcus equation has been widely used in organic charge transport,[8,21–24] we show the corresponding results in Fig. 9 and 10 for comparison. We can see that the results from eqn (12) and eqn (B10) in Appendix B are much larger than those from the Marcus equation at low temperatures in both figures, which has been attributed to the nuclear tunneling effect.[14] It should be mentioned that Jortner et al. have proposed rate expressions that can consider the quantum effect of one or two effective high-frequency molecular modes,[73,74] but our previous work has found that the way to define one or two effective modes is quite arbitrary for transport properties when using the method of Jortner et al.[26]

The charge mobilities are shown in Fig. 11 and 12 for the sexithiophene crystal structures in the HT and LT phases,
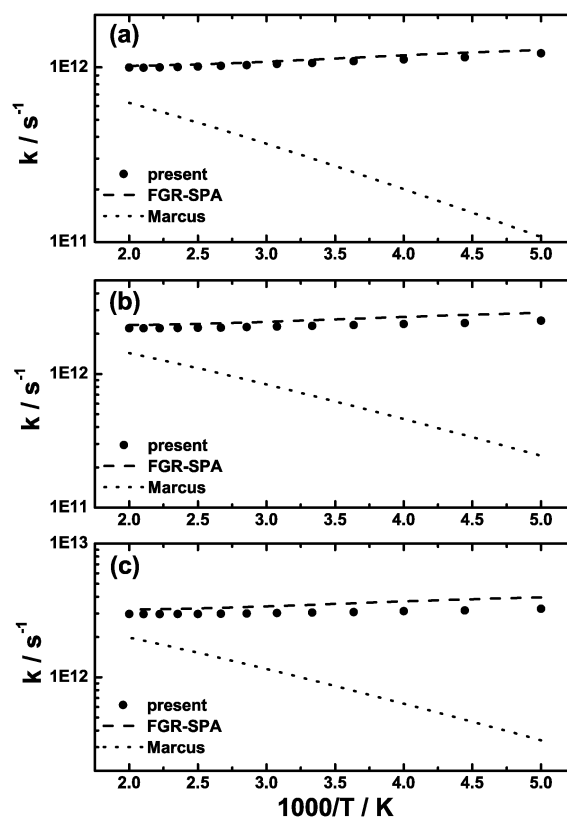


**Fig. 10** The CT rates along the pathways 3, 4 and 5 of the sexithiophene crystal structure in LT phase: (a) for pathway 3; (b) for pathway 4; (c) for pathway 5. The solid circles represent the present results; the dashed line represents the FGR-SPA results; the dotted line represents the Marcus results. By symmetry, pathway 1 is the same as 5, 2 is the same as 4, and 3 is the same as 6.
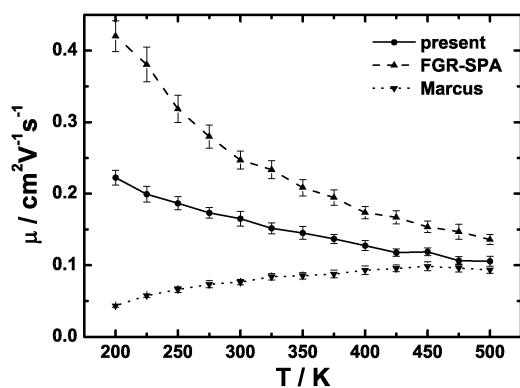
**Fig. 11** The hole mobility as a function of temperature in the HT phase of the sexithiophene crystal structure. The solid line (with circles) are the results from the present CT rates; the dashed line (with upward-pointing triangles) are the results from the FGR-SPA CT rates; the dotted line (with downward-pointing triangles) are the results from the Marcus CT rates.
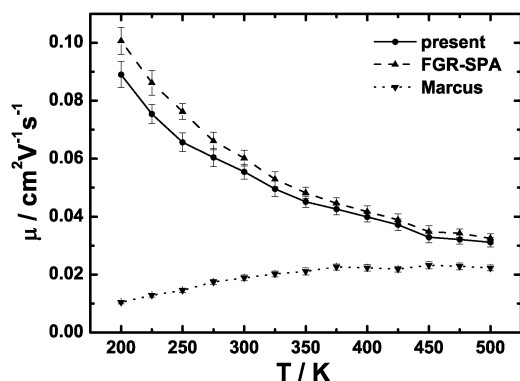


**Fig. 12** The hole mobility as a function of temperature in the LT phase of the sexithiophene crystal structure. The solid line (with circles) are the results from the present CT rates; the dashed line (with upward-pointing triangles) are the results from the FGR-SPA CT rates; the dotted line (with downward-pointing triangles) are the results from the Marcus CT rates.

respectively. Since the present CT rates are smaller than the FGR-SPA results along all the transport directions in Fig. 9 and 10, the present mobilities are smaller than those from the FGR-SPA. However, the mobility *versus* temperature is rather different in both figures. In Fig. 11, the present mobility is about half of the FGR-SPA result at 200 K, and becomes about two-thirds of the latter at room temperature. When temperature reaches 500 K, the present mobility is still significantly smaller than the FGR-SPA result. The above results show that the effect of the strong electronic coupling has to be considered in the HT-phase sexithiophene crystal structure. In Fig. 12, however, the present mobilities are only slightly smaller than the FGR-SPA results at low temperatures, and become almost the same above 400 K. The non-perturbative effect of strong electronic coupling is greatly reduced when the molecular packing is changed from Fig. 3(a) to Fig. 3(b). Therefore, the first-order perturbation should be used with caution for investigating the charge transport in organic semiconductor materials. When the

present mobilities are compared with those based on the Marcus CT rates, we can see that for the sexithiophene crystal structure in the HT phase, the former are obviously larger than the latter below 400 K and approach the latter above 450 K, while for the LT phase, the former are always significantly larger than the latter below 500 K. Thus, the Marcus equation is hardly applicable for these two crystal structures in the investigated temperature region. Moreover, we emphasize that the present mobilities are less dependent on the temperature in Fig. 11 than in Fig. 12. This can be understood from molecular solid-state packing. In the HT phase, the molecular packing along pathways 1, 2, 4 and 5 leads to a bonding or antibonding interaction between adjacent molecules and thus larger transfer integrals. These transfer integrals in the HT phase reduce the CT rates much more than those in the LT phase, especially in the low-temperature region. Thus, the CT rates become much less dependent on the temperature in the HT phase. When the mobilities are simulated with these CT rates along all directions, the temperature dependence of mobilities will also be affected. This can be easily understood if the isotropic diffusion is assumed, and then the diffusion coefficient is approximated as $D \approx \frac{1}{4}\sum_{j} d_j^2 k_j p_j$ where $d_j$, $k_j$ and $p_j$ are the center-to-center hopping distance, CT rate and hopping probability along the $j$-th direction, respectively.[21,75] It is obvious that the temperature dependence of CT rates largely decides the temperature dependence of mobilities. As the CT rates in HT phase are reduced much more in the low-temperature region, the simulated mobilities become less dependent on the temperature.

In fact, grains and grain boundaries are always present in actual OTFTs. As the grain size increases, the number of grain boundaries decreases. Previous work on sexithiophene has shown that the temperature dependence of mobility changes drastically from small grains, where mobility is thermally activated, to larger grains, for which mobility becomes practically temperature-independent,[47] so we can say that the grain boundaries could be responsible for the charge mobility to be thermally activated. In our present model, the grain size can be regarded as infinitely large, and so there are no grain boundaries. If grain boundaries are present, depending on the grain size, the present mobility could be temperature-independent or thermally activated, especially for HT-phase sexithiophene. With the grain boundary being considered, the thermally activated hopping transport mechanism could also be used to explain the temperature-independent transport in pentacene thin-film transistors[76] when the nuclear tunneling effect and nonperturbative effect of electronic coupling are considered at the same time. However, there are difficulties in using the semiclassical Marcus CT formula to explain these experimental phenomena.

## V. Conclusion

To summarize, we apply a quantum CT rate theory without weak coupling assumption to investigate the influence of the molecular packing for charge transport properties in organic semiconductor materials. Sexithiophene crystal structures in the HT and LT phases are exemplified to show that the present method is feasible and can be used to investigate the

applicability of the first-order perturbation, although the errors introduced by the SPA approximation are still difficult to estimate. Comparing the present results with the FGR-SPA results, we find that, in the strong electronic coupling case, the charge mobilities can be significantly smaller than those obtained with the first-order perturbation, especially in the low-temperature region. As the molecular packing varies from the LT phase to the HT phase of sexithiophene crystal structures, the mobilities become less dependent on temperature. We conclude that the molecular packing in HT phase leads to the bonding or antibonding interaction along some transport directions, which strengthens the nonperturbative effect of the electronic coupling. When the grain boundaries are considered, the thermally activated hopping transport mechanism can be used to explain the temperature-independent charge mobility from the present quantum CT rate theory with the kinetic Monte-Carlo simulation of charge mobility.

Recently, the dynamic disorder in organic semiconductor materials has received much attention,[77–79] and the CT rates based on first-order perturbation have been employed.[22,60] It has been observed that the electronic coupling can increase significantly as a result of thermal vibrations, but the nonperturbative effect of the electronic coupling has not been considered in these studies. The present work indicates that the nonperturbative effect of strong electronic coupling may become important in cases with large intermolecular couplings. The method presented in this paper has the merit of rapid computation and opens up possibilities towards this goal.

## Acknowledgements

## References

1 A. R. Murphy and J. M. J. Fréchet, Chem. Rev., 2007, 107, 1066.
2 C. D. Dimitrakopoulos and P. R. L. Malenfant, Adv. Mater., 2002, 14, 99.
3 S. C. Lo and P. L. Burn, Chem. Rev., 2007, 107, 1097.
4 H. Spanggaard and F. C. Krebs, Sol. Energy Mater. Sol. Cells, 2004, 83, 125.
5 J. L. Brédas, D. Beljonne, V. Coropceanu and J. Cornil, Chem. Rev., 2004, 104, 4971.
6 V. Coropceanu, J. Cornil, D. A. da Silva Filho, Y. Olivier, R. Silbey and J. L. Brédas, Chem. Rev., 2007, 107, 926.
7 L. Antolini, G. Horowitz, F. Kouki and F. Garnier, Adv. Mater., 1998, 10, 382.
8 X. D. Yang, L. J. Wang, C. L. Wang, W. Long and Z. G. Shuai, Chem. Mater., 2008, 20, 3205.
9 Z. Rang, A. Haraldsson, D. M. Kim, P. P. Ruden, M. I. Nathan, R. J. Chesterfield and C. D. Frisbie, Appl. Phys. Lett., 2001, 79, 2731.
10 C. Goldmann, S. Haas, C. Krellner, K. P. Pernstich, D. J. Gundlach and B. Batlogg, J. Appl. Phys., 2004, 96, 2080.
11 V. C. Sundar, J. Zaumseil, V. Podzorov, E. Menard, R. L. Willett, T. Someya, M. E. Gershenson and J. A. Rogers, Science, 2004, 303, 1644.
12 V. Podzorov, E. Menard, A. Borissov, V. Kiryukhin, J. A. Rogers and M. E. Gershenson, Phys. Rev. Lett., 2004, 93, 086602.
13 V. Podzorov, E. Menard, J. A. Rogers and M. E. Gershenson, Phys. Rev. Lett., 2005, 95, 226601.
14 G. J. Nan, X. D. Yang, L. J. Wang, Z. G. Shuai and Y. Zhao, Phys. Rev. B: Condens. Matter Mater. Phys., 2009, 79, 115203.
15 D. A. da Silva Filho, E. G. Kim and J. L. Brédas, Adv. Mater., 2005, 17, 1072.
16 F. J. M. Hoeben, P. Jonkheijm, E. W. Meijer and A. P. H. J. Schenning, Chem. Rev., 2005, 105, 1491.
17 J. D. Dunitz and A. Gavezzotti, Acc. Chem. Res., 1999, 32, 677.
18 J. D. Dunitz and A. Gavezzotti, Chem. Soc. Rev., 2009, 38, 2622.
19 Y. C. Cheng, R. J. Silbey, D. A. da Silva Filho, J. P. Calbert, J. Cornil and J. L. Brédas, J. Chem. Phys., 2003, 118, 3764.
20 N. Karl, J. Marktanner, R. Stehle and W. Warta, Synth. Met., 1991, 42, 2473.
21 W. Q. Deng and W. A. Goddard III, J. Phys. Chem. B, 2004, 108, 8614.
22 N. G. Martinelli, Y. Olivier, S. Athanasopoulos, M. R. Delgado, K. R. Pigg, D. A. da Silva Filho, R. S. Sánchez-Carrera, E. Venuti, R. G. Della Valle, J. L. Brédas, D. Beljonne and J. Cornil, ChemPhysChem, 2009, 10, 2265.
23 G. R. Hutchison, M. A. Ratner and T. J. Marks, J. Am. Chem. Soc., 2005, 127, 16866.
24 Y. B. Song, C. A. Di, X. D. Yang, S. P. Li, W. Xu, Y. Q. Liu, L. M. Yang, Z. G. Shuai, D. Q. Zhang and D. B. Zhu, J. Am. Chem. Soc., 2006, 128, 15940.
25 M. Malagoli and J. L. Brédas, Chem. Phys. Lett., 2000, 327, 13.
26 G. J. Nan, L. J. Wang, X. D. Yang, Z. G. Shuai and Y. Zhao, J. Chem. Phys., 2009, 130, 024704.
27 W. H. Miller, S. D. Schwartz and J. W. Tromp, J. Chem. Phys., 1983, 79, 4889.
28 M. Topaler and N. Makri, Chem. Phys. Lett., 1993, 210, 285.
29 H. B. Wang, X. Sun and W. H. Miller, J. Chem. Phys., 1998, 108, 9726.
30 M. Topaler and N. Makri, J. Phys. Chem., 1996, 100, 4430.
31 I. R. Craig, M. Thoss and H. B. Wang, J. Chem. Phys., 2007, 127, 144503.
32 L. P. Chen and Q. Shi, J. Chem. Phys., 2009, 130, 134505.
33 R. P. Feynman and A. R. Hibbs, Quantum Mechanics and Path Integrals, McGraw-Hill, New York, 1965.
34 C. H. Mak and D. Chandler, Phys. Rev. A: At., Mol., Opt. Phys., 1990, 41, 5709.
35 D. Thirumalai and B. J. Berne, J. Chem. Phys., 1983, 79, 5029.
36 J. S. Bader, R. A. Kuharski and D. Chandler, J. Chem. Phys., 1990, 93, 230.
37 W. H. Miller, J. Chem. Phys., 1975, 62, 1899.
38 A. A. Golosov and D. R. Reichman, J. Chem. Phys., 2003, 118, 457.
39 W. H. Miller, J. Chem. Phys., 1971, 55, 3146.
40 P. G. Wolynes, J. Chem. Phys., 1987, 87, 6559.
41 S. L. Yang and J. S. Cao, J. Chem. Phys., 2005, 122, 094108.
42 W. H. Miller, Y. Zhao, M. Ceotto and S. Yang, J. Chem. Phys., 2003, 119, 1329.
43 J. S. Cao, L. W. Ungar and G. A. Voth, J. Chem. Phys., 1996, 104, 4189.
44 J. Cornil, J. P. Calbert, D. Beljonne, R. Silbey and J. L. Brédas, Adv. Mater., 2000, 12, 978.
45 T. Siegrist, C. Kloc, R. A. Laudise, H. E. Katz and R. C. Haddon, Adv. Mater., 1998, 10, 379.
46 S. Nagamatsu, K. Kaneto, R. Azumi, M. Matsumoto, Y. Yoshida and K. Yase, J. Phys. Chem. B, 2005, 109, 9374.
47 G. Horowitz and M. E. Hajlaoui, Adv. Mater., 2000, 12, 1046.
48 T. Siegrist, R. M. Fleming, R. C. Haddon, R. A. Laudise, A. J. Lovinger, H. E. Katz, P. Bridenbaugh and D. D. Davis, J. Mater. Res., 1995, 10, 2170.
49 G. Horowitz, B. Bachet, A. Yassar, P. Lang, F. Demanze, J. L. Fave and F. Garnier, Chem. Mater., 1995, 7, 1337.
50 J.D. Andersen, C. B. Duke and V. M. Kenkre, Phys. Rev. Lett., 1983, 51, 2202.
51 Y. Zhao, W. Z. Liang and H. Nakamura, J. Phys. Chem. A, 2006, 110, 8204.
52 A. J. Leggett, S. Chakravarty, A. T. Dorsey, M. P. A. Fisher, A. Garg and W. Zwerger, Rev. Mod. Phys., 1987, 59, 1.
53 H. B. Wang, X. Y. Song, D. Chandler and W. H. Miller, J. Chem. Phys., 1999, 110, 4828.
54 L. Mühlbacher and R. Egger, J. Chem. Phys., 2003, 118, 179.

55 Q. Shi, L. P. Chen, G. J. Nan, R. X. Xu and Y. J. Yan, *J. Chem. Phys.*, 2009, **130**, 164518.
56 R. Kubo and Y. Toyozawa, *Prog. Theor. Phys.*, 1955, **13**, 160.
57 J. J. Markham, *Rev. Mod. Phys.*, 1959, **31**, 956.
58 P. Siders and R. A. Marcus, *J. Am. Chem. Soc.*, 1981, **103**, 741.
59 R. P. Feynman, *Statistical Mechanics*, ed. W. A. Benjamin, Reading, Massachusetts, 1972.
60 L. J. Wang, Q. K. Li, Z. G. Shuai, L. P. Chen and Q. Shi, *Phys. Chem. Chem. Phys.*, 2010, **12**, 3309.
61 J. R. Reimers, *J. Chem. Phys.*, 2001, **115**, 9103.
62 J. Cornil, D. Beljonne, J. P. Calbert and J. L. Brédas, *Adv. Mater.*, 2001, **13**, 1053.
63 X. Y. Li, *J. Comput. Chem.*, 2001, **22**, 565.
64 E. F. Valeev, V. Coropceanu, D. A. da Silva Filho, S. Salman and J. L. Brédas, *J. Am. Chem. Soc.*, 2006, **128**, 9882.
65 T. Fujita, H. Nakai and H. Nakatsuji, *J. Chem. Phys.*, 1996, **104**, 2410.
66 A. Troisi and G. Orlandi, *Chem. Phys. Lett.*, 2001, **344**, 509.
67 J. S. Huang and M. Kertesz, *Chem. Phys. Lett.*, 2004, **390**, 110.
68 M. J. Frisch, G. W. Trucks, H. B. Schlegel, G. E. Scuseria, M. A. Robb, J. R. Cheeseman, J. A. Montgomery, T. Vreven, K. N. Kudin, J. C. Burant, J. M. Millam, S. S. Iyengar, J. Tomasi, V. Barone, B. Mennucci, M. Cossi, G. Scalmani, N. Rega, G. A. Petersson, H. Nakatsuji, M. Hada, M. Ehara, K. Toyota, R. Fukuda, J. Hasegawa, M. Ishida, T. Nakajima, Y. Honda, O. Kitao, H. Nakai, M. Klene, X. Li, J. E. Knox, H. P. Hratchian, J. B. Cross, V. Bakken, C. Adamo, J. Jaramillo, R. Gomperts, R. E. Stratmann, O. Yazyev, A. J. Austin, R. Cammi, C. Pomelli, J. W. Ochterski, P. Y. Ayala, K. Morokuma, G. A. Voth, P. Salvador, J. J. Dannenberg, V. G. Zakrzewski, S. Dapprich, A. D. Daniels, M. C. Strain, O. Farkas, D. K. Malick, A. D. Rabuck, K. Raghavachari, J. B. Foresman, J. V. Ortiz, Q. Cui, A. G. Baboul, S. Clifford, J. Cioslowski, B. B. Stefanov, G. Liu, A. Liashenko, P. Piskorz, I. Komaromi, R. L. Martin, D. J. Fox, T. Keith, M. A. Al-Laham, C. Y. Peng, A. Nanayakkara, M. Challacombe, P. M. W. Gill, B. Johnson, W. Chen, M. W. Wong, C. Gonzalez and J. A. Pople, *GAUSSIAN 03 (Revision E01)*, Gaussian, Inc., Wallingford CT, 2004.
69 E. D. Donato, R. P. Fornari, S. D. Motta, Y. Li, Z. H. Wang and F. Negri, *J. Phys. Chem. B*, 2010, **114**, 5327.
70 A. Dodabalapur, L. Torsi and H. E. Katz, *Science*, 1995, **268**, 270.
71 P. Ostoja, S. Guerri, S. Rossini, M. Servidori, C. Taliani and R. Zamboni, *Synth. Met.*, 1993, **54**, 447.
72 Y. Zhao, G. Mil'nikov and H. Nakamura, *J. Chem. Phys.*, 2004, **121**, 8854.
73 J. Ulstrup and J. Jortner, *J. Chem. Phys.*, 1975, **63**, 4358.
74 J. Jortner, *J. Chem. Phys.*, 1976, **64**, 4860.
75 L. J. Wang, G. J. Nan, X. D. Yang, Q. Peng, Q. K. Li and Z. G. Shuai, *Chem. Soc. Rev.*, 2010, **39**, 423.
76 S. F. Nelson, Y.-Y. Lin, D. J. Gundlach and T. N. Jackson, *Appl. Phys. Lett.*, 1998, **72**, 1854.
77 A. Troisi and G. Orlandi, *J. Phys. Chem. A*, 2006, **110**, 4065.
78 A. Troisi and G. Orlandi, *Phys. Rev. Lett.*, 2006, **96**, 086601.
79 D. P. McMahon and A. Troisi, *ChemPhysChem*, 2010, **11**, 2067.
80 J. S. Cao and G. A. Voth, *J. Chem. Phys.*, 1997, **106**, 1769.
81 S. H. Lin, C. H. Chang, K. K. Liang, R. Chang, Y. J. Shiu, J. M. Zhang, T. S. Yang, M. Hayashi and F. C. Hsu, *Adv. Chem. Phys.*, 2002, **121**, 1.
82 D. Chandler, *Theory of quantum processes in liquids*, in *Les Houches, Session L1, Liquids Freezing and Glass Transition*, ed. J. P. Hansen, D. Levesque and J. Zinn-Justin, Elsevier Science Publishers B. V., North Holland, 1991.